Operational Principles of Three-Phase Single Active Bridge DC/DC Converters Under Duty Cycle Control

Yu Sang, *Student Member, IEEE*, Adrià Junyent-Ferré, *Senior Member, IEEE*, and Tim C. Green, *Fellow, IEEE*

***Abstract*—Single active bridge (SAB) dc/dc converters are attractive options for unidirectional dc/dc conversion in future medium power generation applications, offering galvanic isolation and a diode-based output side. SAB dc/dc converters must be controlled by adjusting the active bridge switching duty cycle, unlike dual active bridge converters where the phase-shift angle control is normally used. This article presents a comprehensive analysis of the operational principles of three-phase SAB dc/dc converters that arise from different duty cycle operation ranges. Moreover, the converter performances such as transformer harmonic currents are analyzed and compared between different input and output dc voltage conditions. Finally, an experimental validation using a small-scale prototype is presented.**

***Index Terms*—Duty cycle control, operational modes, performances, three-phase single active bridge (3p-SAB) dc/dc converter.**

I. Introduction

ISOLATED dc/dc converters are widely applied in many energy conversion applications, thanks to the galvanic isolation, high step-up ratios, compact design, and high efficiency [1]–[6]. Two converter types: dual active bridge (DAB) converters [7]–[13] and single active bridge (SAB) converters [7], [14]–[19] are the most popular converter choices among all isolated dc/dc converters. An isolated dc/dc converter normally combines two converter bridges and an intermediate transformer, and it can be designed single phase [7]–[10], [14]–[16] or three phase [11]–[13], [17]–[19].

Figs. 1 and 2 show the general topology of DAB and SAB converters. It can be seen that they share many similarities, but the main difference is that the DAB converter has two controllable bridges on both sides, while the SAB converter comprises of a controllable active bridge on the primary side and a passive diode based rectifier on the secondary side. The less expensive passive bridge not only reduces the volume and cost, but can use a series connection to obtain a higher voltage rating. These characteristics make SAB converters more attractive for medium voltage (MV) applications such as dc wind farms [20], [21].

Manuscript received August 22, 2019; revised December 2, 2019; accepted January 4, 2020. Date of publication January 7, 2020; date of current version April 22, 2020. Recommended for publication by Associate Editor J. Biela. *(Corresponding author: Yu Sang.)*

The authors are with Electrical and Electronic Engineering, Imperial College London, London SW7 2AZ, U.K. (e-mail: y.sang15@imperial.ac.uk; adria.junyent-ferre@imperial.ac.uk; t.green@imperial.ac.uk).

Color versions of one or more of the figures in this article are available online at https://ieeexplore.ieee.org.

Digital Object Identifier 10.1109/TPEL.2020.2964901

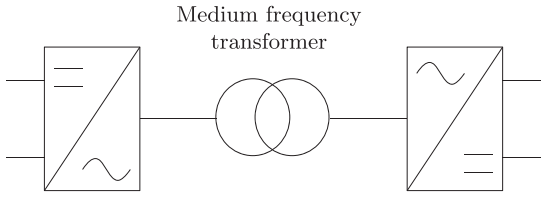

Fig. 1. General topology of dual active bridge converters.

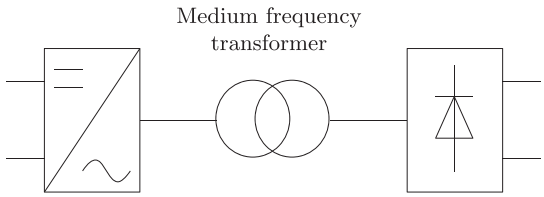

Fig. 2. General topology of single active bridge converters.

In DAB converters, the converter power flow is controlled via phase shift (PS) angle control given the constant two side dc voltages [22]. Other advanced PS control methods such as dual-phase-shift [2], extended-phase-shift [23], and triple-phase-shift [24] are also proposed to improve the efficiency or reduce the transformer reactive power. However, in SAB converters only the active bridge duty cycle [14], [25] can be independently changed and the power can only be transferred from the active to the passive bridge. Thus, it is suggested to use the duty cycle as the control variable and this method is called duty cycle control.

There have already been many studies about the operational principles of DAB converters including single-phase DAB (1p-DAB) [12] and three-phase DAB (3p-DAB) [13] converters under different PS control methods. There are also some studies about the operation of single phase SAB (1p-SAB) converters [14], [15]. However, when moving to three-phase SAB (3p-SAB) converters, only a few papers about the operation of 3p-SAB converters could be found [17]–[19]. Jacobs *et al.* [17] and Garcia-Bediaga *et al.* [18] present the current and power equations under the basic operation when the active duty cycle keeps at 0.5. Sommer *et al.* [19] present the discontinuous mode when the 3p-SAB uses a delta-wye transformer arrangement, but does not consider the comprehensive operational principles with the most common wye–wye transformer arrangement.

Even though the 3p-SAB converters require more components, they show advantages over 1p-SAB in four aspects. First, the current stress would be reduced given the same power rating and it is advantageous for high-power applications [18]. Second,

as there are more phases, the dc currents would be smoother so that less dc capacitance is required [7], [17], [26]. Third, further increasing the number of phases would not be feasible due to converter cost or volume, and 3p-SAB converters can achieve a higher efficiency, as recommended in [27]. Fourth, because of the inherent redundancy, it has been suggested that if a fault affected one phase, the other two phases could still be used to operate under a reduced power set-point, rather than having a full outage. Therefore, the 3p-SAB converters are regarded as a promising future converter solution and are chosen as the research target in this article.

In 3p-SAB converters, when the active duty cycle d_1 varies, the passive diode bridge duty cycle d_2 and PS Δ_d are also affected. It is not straightforward to obtain the operational relationships among them. The transformer voltage waveforms under changing duty cycle for 3p-SAB converters should be analyzed first. Then, the current equations with different combinations of voltages can be obtained and solved, based on which the converter operational principles could be revealed. Furthermore, the transformer voltages and currents may change significantly with the duty cycle [28], and should be investigated thoroughly in order to provide insights for the converter design.

Therefore, this article intends to mitigate the knowledge gap in operational principles of the 3p-SAB converters and provides an extensive analysis of this topic. It is found that when the (active bridge) duty cycle is changed from 0 to 0.5, there are eight modes, which also depend on the ratio between the primary and secondary dc voltages. Based on the operational principles derived, the converter performance is compared under two different voltage conditions, in order to provide insights into the effect of parameters on converter design. Finally, experimental validations are performed.

The rest of this article is structured as follows. Section II defines the variables that are used in this article and Section III presents the voltage shapes of 3p-SAB converters under duty cycle control. Sections IV and V then separate the converter operation into high and low-voltage conditions, and list the transformer current equations under different operational modes. On the basis of the operational principles, the evaluations of converter power flow, transformer voltage and current, input and output current harmonics are given in Section VI. Theses operational principles and performance evaluations are verified by experimental results in Section VII. Section VIII discusses the findings and concludes this article.

II. Converter Description

The detailed circuit topology of a 3p-SAB converter is illustrated in Fig. 3, where the three-phase transformer uses the wye–wye configuration on the primary and secondary side. $S_1 \sim S_6$ represent the active bridge switches, and $D_1 \sim D_6$ represent the passive bridge diodes. L_s is the equivalent series inductance of the transformer in each phase, and the resistance is usually small enough to be ignored. It is suggested to use the transformer leakage inductance as the series inductance, in order to make the converter more compact and efficient [29]. $U_{\rm dc1}$ and $U_{\rm dc2}$ are the dc voltages on the primary side and secondary side.

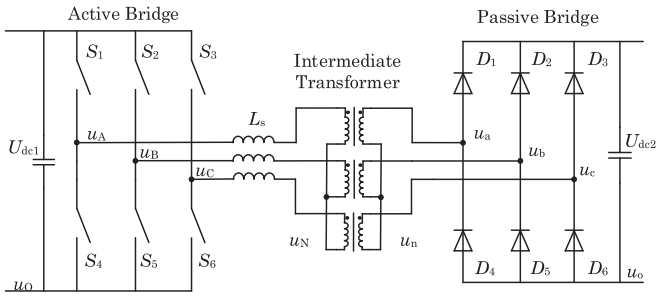

Fig. 3. Circuit topology of a 3p-SAB converter.

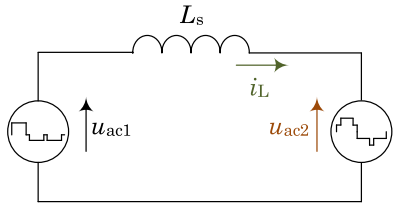

Fig. 4. Equivalent circuit for each phase of the transformer in 3p-SAB converters.

The transformer turn-ratio is n so the secondary dc voltage that is referred to the primary side is $U'_{\rm dc2} = U_{\rm dc2}/n$. The dc voltage conversion ratio (DVCR) [30] is defined as: $m = U'_{\rm dc2}/U_{\rm dc1}$. It is assumed that the switches and diodes are ideal and nonlinear effects of the transformer are ignored.

Since the three phases are symmetric, only one phase needs to be analyzed. The equivalent circuit topology of each phase in the wye–wye connected three-phase transformer is shown in Fig. 4, where $u_{\rm ac1}$ and $u_{\rm ac2}$ are the transformer phase voltages, which are also the middle-to-neutral voltages $u_{\rm ac1} = u_{\rm AN}, u_{\rm BN}, u_{\rm CN}$ and $u_{\rm ac2} = u_{\rm an}, u_{\rm bn}, u_{\rm cn}$ in Fig. 3.

In steady states, $u_{\rm ac1}$ and $u_{\rm ac2}$ are fixed and they determine the shape and value of transformer currents, respectively. However, $u_{\rm ac1}$ and $u_{\rm ac2}$ depend on the duty cycles and may have three or four stages. Furthermore, different combinations of transformer phase voltages make the transformer phase current i_L have even more intervals and unique shapes. Therefore, the converter/transformer voltages are analyzed first in the next section, followed by the detailed operational principles in Sections IV and V.

III. Converter Voltages

Transformer phase voltages in 3p-SAB converters are determined by the primary and secondary duty cycle d_1 and d_2. Due to symmetry, when the duty cycle $d_1(d_2)$ is larger than 0.5, the produced current and voltages are the inverse (flipped over around x-axis) of those under $1 - d_1(d_2)$ which is smaller than 0.5. Therefore, only the duty cycles that are smaller than 0.5 are analyzed in this article

Under different duty cycles, the transformer neutral point voltages $u_{\rm NO}$ and $u_{\rm no}$ are different and nonzero. Consequently, ac voltages $u_{\rm ac1}$ and $u_{\rm ac2}$ may have zero stages or not. If the duty cycle is larger than 1/3, then the bridge middle point voltages have overlaps, and $u_{\rm ac1}$ and $u_{\rm ac2}$ would never be zero. This

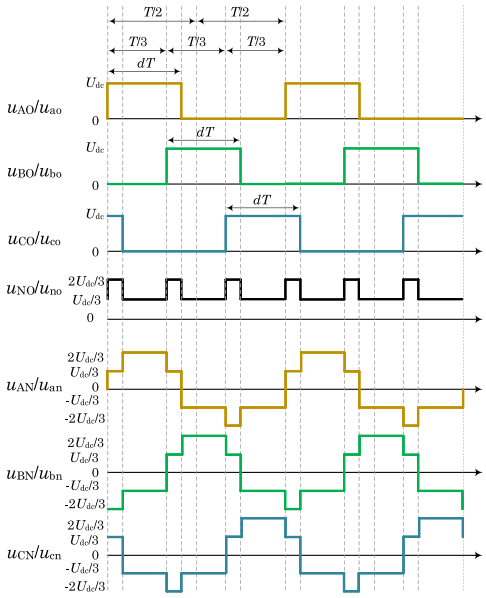

Fig. 5. Bridge middle point voltages, transformer neutral point voltages, and middle-to-neutral voltages under large duty cycle (>1/3) for 3p-SAB converters.

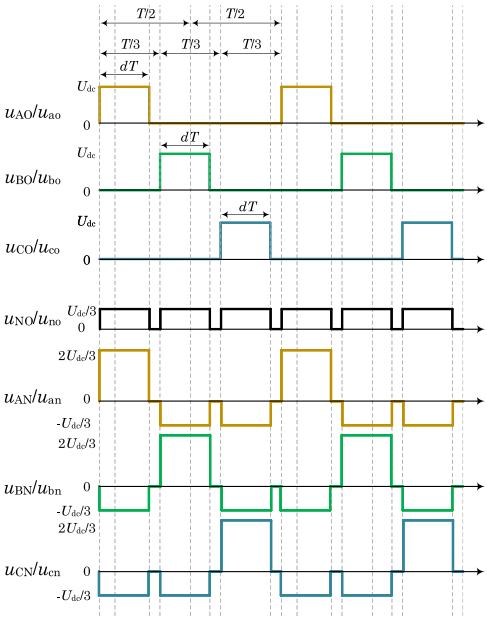

Fig. 6. Bridge middle point voltages, transformer neutral point voltages, and middle-to-neutral voltages under small duty cycle (≤1/3) for 3p-SAB converters.

condition is shown in Fig. 5 with the bridge middle point voltages, transformer neutral point voltages, and middle-to-neutral voltages. However, when the duty cycle is smaller than 1/3, the bridge middle point voltages do not have overlaps, and $u_{\rm ac1}$ and $u_{\rm ac2}$ would have zero stages. This condition is depicted in Fig. 6.

Figs. 5 and 6 can represent both the active bridge and the passive bridge voltages, which means $U_{\rm dc}$ can be $U_{\rm dc1}$ or $U'_{\rm dc2}$. The active bridge duty cycle d_1 is controllable which means $u_{\rm ac1}$ is controllable. However, as mentioned before, the secondary bridge duty cycle d_2 and voltage $u_{\rm ac2}$ can not be independently controlled. Instead, they are controlled by the transformer phase current if the dc voltages are constant. Moreover, the PS Δ_d between two bridges is also not independently controllable. If d_1, d_2, and Δ_d are all decided, the transformer phase current i_L is decided and the converter power, turn-OFF current, and peak current can be obtained.

There exists only one relationship between d_1, d_2, and Δ_d, given fixed m and d_1. In order to find this relationship, different combinations of d_1, d_2, and Δ_d are tried, and the only feasible solution can be obtained. It is found that the relationships are different for the high DVCR scenario when $m \geq 1/2$ and for the low DVCR scenario when $m < 1/2$, because the PS may be larger than 1/6 of a period under low DVCR scenarios. Moreover, in each DVCR scenario, when the duty cycle is in different subranges of [0, 0.5], the current equations and the solved d_2 and Δ_d may be different. Four operational modes are found under each DVCR scenario and they are concluded as the operational principles in the next two sections.

IV. Operational Principles of 3p-SAB Converters Under High DVCR Conditions

Four operating modes are found out when d_1 is in the range of [0, 0.5] under high DVCR conditions ($m = U'_{\rm dc2}/U_{\rm dc1} \geq 1/2$). There are three continuous current modes and one discontinuous current mode (DCM), in which "continuous" means the transformer ac current is continuous without staying at zero. In total, there are 12 intervals in the continuous modes and nine intervals exist in the discontinuous mode.

A. Continuous Current Mode 1

When the value of d_1 is large and in the range of $[\frac{2U_{\rm dc1}-U'_{\rm dc2}}{3U_{\rm dc1}}, \frac{1}{2}]$, the converter works in Continuous Current Mode 1 (CCM1) as shown in Fig. 7. There are 12 intervals and in each interval, the slope of the linear phase current equation is determined by the difference between $u_{\rm ac1}$ and $u_{\rm ac2}$.

In interval $t_0 \sim t_1$, the upper switch of phase A turns on but because i_A is negative, the lower switch of phase a is still conductive and will not turn off until t_1. In interval $t_1 \sim t_2$, the upper switch of phase a turns on so the rate of change of current is reduced. In interval $t_2 \sim t_3$, the upper switch of phase C turns off, but the transformer current i_C is still positive so the upper switch of phase c is still conductive and will not change until t_3. In interval $t_3 \sim t_4$, the upper switch of phase c turns off and this interval continues until at t_4 the upper switch of phase B turns on. The rest of intervals are similar to the above process, but the commutations happen among phase B/b/A/a and C/c/B/b. The rate of change of transformer phase current is always the difference between $u_{\rm ac1}$ and $u_{\rm ac2}$ and all current equations are given in Table I.

Since the three phases are symmetric, $i_A + i_B + i_C = 0$ and $i_A = i_B(t - T/3) = i_C(t + T/3)$, the symmetric current conditions are obtained in (1) and the last four currents $i_8 \sim i_{11}$ can be calculated based on the first eight currents $i_0 \sim i_7$

$$\begin{aligned} i_0 + i_4 + i_8 &= 0 \\ i_1 + i_5 + i_9 &= 0 \\ i_2 + i_6 + i_{10} &= 0 \\ i_3 + i_7 + i_{11} &= 0 \end{aligned} \tag{1}$$

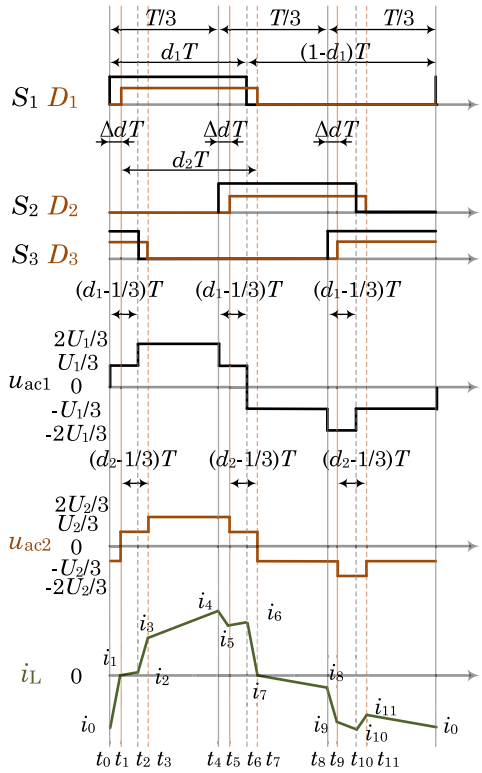

Fig. 7. Waveforms of 3p-SAB converters in CCM1 under high DVCR conditions.

At t_1 and t_7, the transformer current crosses zero so the zero current conditions are

$$i_1 = 0, \quad i_7 = 0. \tag{2}$$

The other six currents i_0, $i_2 \sim i_6$, two switch state variables d_2 and Δ_d need to be solved, and the first eight equations in Table I are independent. As a result, variables can be solved and the results are given as (3)–(5). For the sake of brevity, only i_0 is shown here and the rest currents can be derived using Table I

$$i_0 = -\frac{T_s}{9L_s}\frac{(U_{\rm dc1} - U'_{\rm dc2})(U'_{\rm dc2} + U_{\rm dc1})}{U_{\rm dc1}} \tag{3}$$

$$d_2 = d_1 \tag{4}$$

$$\Delta_d = \frac{U_{\rm dc1} - U'_{\rm dc2}}{3U_{\rm dc1}}. \tag{5}$$

Assuming the converter is lossless, the power flow through the AC-link is calculated as

$$P = \frac{T_s}{9L_s}\frac{U'_{\rm dc2}(U_{\rm dc1} - U'_{\rm dc2})(U_{\rm dc1} + U'_{\rm dc2})}{U_{\rm dc1}}. \tag{6}$$

In this mode, although d_1 is changed, the PS and power flow keep constant, and d_2 has the same value as d_1, in order to keep the power flow fixed.

TABLE I
TRANSFORMER PHASE CURRENT EQUATIONS FOR 3p-SAB CONVERTERS IN CCM1 UNDER HIGH DVCR CONDITIONS

Intervals	Transformer current i_L equations
$0 \sim t_1$	$i_1 - i_0 = \frac{U_{dc1} + U'_{dc2}}{3L_s} T_s \Delta_d$
$t_1 \sim t_2$	$i_2 - i_1 = \frac{U_{dc1} - U'_{dc2}}{3L_s} T_s (d_1 - \frac{1}{3} - \Delta_d)$
$t_2 \sim t_3$	$i_3 - i_2 = \frac{2U_{dc1} - U'_{dc2}}{3L_s} T_s (d_2 - d_1 + \Delta_d)$
$t_3 \sim t_4$	$i_4 - i_3 = \frac{2U_{dc1} - 2U'_{dc2}}{3L_s} T_s (-d_2 + \frac{2}{3} - \Delta_d)$
$t_4 \sim t_5$	$i_5 - i_4 = \frac{U_{dc1} - 2U'_{dc2}}{3L_s} T_s \Delta_d$
$t_5 \sim t_6$	$i_6 - i_5 = \frac{U_{dc1} - U'_{dc2}}{3L_s} T_s (d_1 - \frac{1}{3} - \Delta_d)$
$t_6 \sim t_7$	$i_7 - i_6 = \frac{-U_{dc1} - U'_{dc2}}{3L_s} T_s (d_2 - d_1 + \Delta_d)$
$t_7 \sim t_8$	$i_8 - i_7 = \frac{-U_{dc1} + U'_{dc2}}{3L_s} T_s (-d_2 + \frac{2}{3} - \Delta_d)$
$t_8 \sim t_9$	$i_9 - i_8 = \frac{-2U_{dc1} + U'_{dc2}}{3L_s} T_s \Delta_d$
$t_9 \sim t_{10}$	$i_{10} - i_9 = \frac{-2U_{dc1} + 2U'_{dc2}}{3L_s} T_s (d_1 - \frac{1}{3} - \Delta_d)$
$t_{10} \sim t_{11}$	$i_{11} - i_{10} = \frac{-U_{dc1} + 2U'_{dc2}}{3L_s} T_s (d_2 - d_1 + \Delta_d)$
$t_{11} \sim T_s$	$i_0 - i_{11} = \frac{-U_{dc1} + U'_{dc2}}{3L_s} T_s (-d_2 + \frac{2}{3} - \Delta_d)$

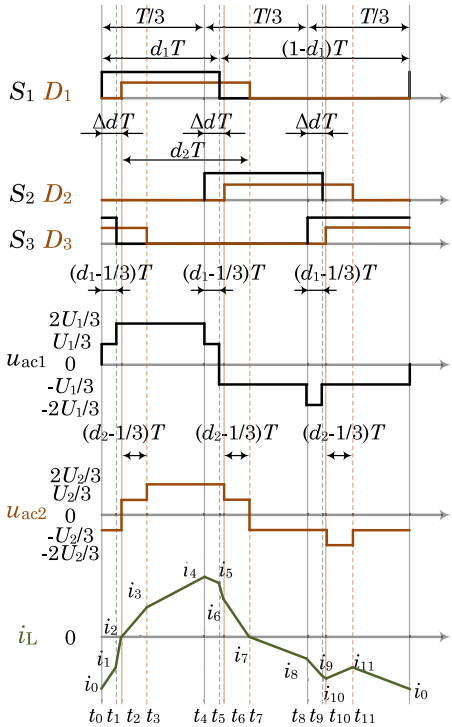

Fig. 8. Waveforms of 3p-SAB converters in CCM2 under high DVCR conditions.

B. Continuous Current Mode 2

When the value of d_1 is in the range of $[\frac{1}{3}, \frac{2U_{\rm dc1} - U'_{\rm dc2}}{3U_{\rm dc1}}]$, the converter works in CCM2 as shown in Fig. 8. There are 12 intervals and current equations are given in Table II.

TABLE II
TRANSFORMER PHASE CURRENT EQUATIONS FOR 3p-SAB CONVERTERS IN CCM2 UNDER HIGH DVCR CONDITIONS

Intervals	Transformer current i_L equations
$0 \sim t_1$	$i_1 - i_0 = \frac{U_{dc1} + U'_{dc2}}{3L_s} T_s(d_1 - \frac{1}{3})$
$t_1 \sim t_2$	$i_2 - i_1 = \frac{2U_{dc1} + U'_{dc2}}{3L_s} T_s(\Delta_d - d_1 + \frac{1}{3})$
$t_2 \sim t_3$	$i_3 - i_2 = \frac{2U_{dc1} - U'_{dc2}}{3L_s} T_s(d_2 - \frac{1}{3})$
$t_3 \sim t_4$	$i_4 - i_3 = \frac{2U_{dc1} - 2U'_{dc2}}{3L_s} T_s(-d_2 + \frac{2}{3} - \Delta_d)$
$t_4 \sim t_5$	$i_5 - i_4 = \frac{U_{dc1} - 2U'_{dc2}}{3L_s} T_s(d_1 - \frac{1}{3})$
$t_5 \sim t_6$	$i_6 - i_5 = \frac{-U_{dc1} - 2U'_{dc2}}{3L_s} T_s(\Delta_d - d_1 + \frac{1}{3})$
$t_6 \sim t_7$	$i_7 - i_6 = \frac{-U_{dc1} - U'_{dc2}}{3L_s} T_s(d_2 - \frac{1}{3})$
$t_7 \sim t_8$	$i_8 - i_7 = \frac{-U_{dc1} + U'_{dc2}}{3L_s} T_s(-d_2 + \frac{2}{3} - \Delta_d)$
$t_8 \sim t_9$	$i_9 - i_8 = \frac{-2U_{dc1} + U'_{dc2}}{3L_s} T_s(d_1 - \frac{1}{3})$
$t_9 \sim t_{10}$	$i_{10} - i_9 = \frac{-U_{dc1} + U'_{dc2}}{3L_s} T_s(\Delta_d - d_1 + \frac{1}{3})$
$t_{10} \sim t_{11}$	$i_{11} - i_{10} = \frac{-U_{dc1} + 2U'_{dc2}}{3L_s} T_s(d_2 - \frac{1}{3})$
$t_{11} \sim T_s$	$i_0 - i_{11} = \frac{-U_{dc1} + U'_{dc2}}{3L_s} T_s(-d_2 + \frac{2}{3} - \Delta_d)$

The symmetric current conditions in (1) also hold. Moreover, at t_2 and t_7, the transformer current crosses zero so the zero current conditions are

$$i_2 = 0, \quad i_7 = 0. \tag{7}$$

The other six currents, d_2 and Δ_d can therefore be solved according to the first 8 equations in Table II. The results are given as (8)–(10). For the sake of brevity, only i_0 is shown here and the rest currents can be derived according to Table II

$$i_0 = -\frac{T_s}{18L_s} \frac{2U_{\rm dc1}^2 + 3U_{\rm dc1}U'_{\rm dc2}d_1 - 2U_{\rm dc1}U'_{\rm dc2} - U'^2_{\rm dc2}}{U_{\rm dc1}} \tag{8}$$

$$d_2 = \frac{3U_{\rm dc1}d_1 - U'_{\rm dc2} + 2U_{\rm dc1}}{6U_{\rm dc1}} \tag{9}$$

$$\Delta_d = \frac{3U_{\rm dc1}d_1 - U'_{\rm dc2}}{6U_{\rm dc1}} \tag{10}$$

Assume the converter is lossless, the power flow through the AC-link is calculated as

$$P = \frac{T_s}{12L_s} \frac{U'_{\rm dc2}(4U_{\rm dc1}^2 d_1 - 3U_{\rm dc1}^2 d_1^2 - U'^2_{\rm dc2})}{U_{\rm dc1}}. \tag{11}$$

In this mode, the converter power, passive duty cycle as well as PS all monotonically increase with the increase of duty cycle.

C. Continuous Current Mode 3

When the value of d_1 is in the range of $[\frac{U'_{\rm dc2}}{3U_{\rm dc1}}, \frac{1}{3}]$, the converter works in CCM3 as shown in Fig. 9. There are 12 intervals and all current equations are given in Table III.

The symmetric current conditions in (1) also hold. Moreover, at t_1 and t_6, the transformer current crosses zero so the zero current conditions are

$$i_1 = 0, \quad i_6 = 0 \tag{12}$$

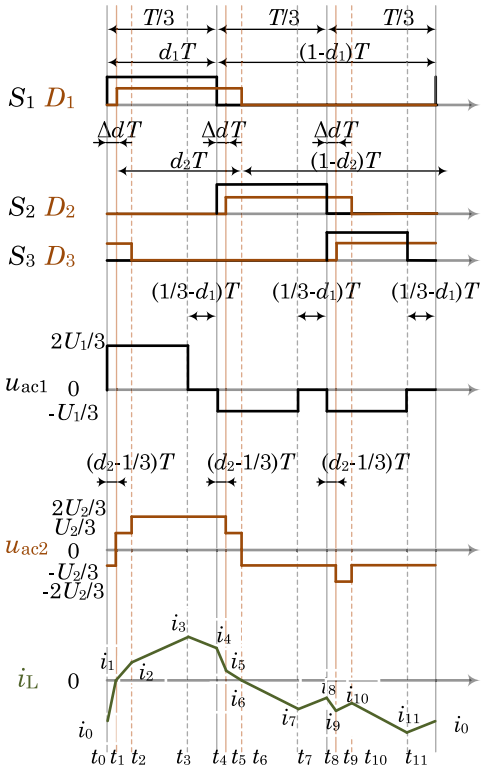

Fig. 9. Waveforms of 3p-SAB converters in CCM3 under high DVCR conditions.

The six currents, d_2 and Δ_d can therefore be solved according to the first 8 equations in Table III. As a result, variables can be solved and the results are given as (13), (14), and (15). For the sake of brevity, only i_0 is shown here and the rest currents can be derived according to Table III

$$i_0 = -\frac{T_s}{18L_s} \frac{(2U_{\rm dc1} + U'_{\rm dc2})(3U_{\rm dc1}d_1 - U'_{\rm dc2})}{U_{\rm dc1}} \tag{13}$$

$$d_2 = \frac{3U_{\rm dc1}d_1 - U'_{\rm dc2} + 2U_{\rm dc1}}{6U_{\rm dc1}} \tag{14}$$

$$\Delta_d = \frac{3U_{\rm dc1}d_1 - U'_{\rm dc2}}{6U_{\rm dc1}}. \tag{15}$$

Assume the converter is lossless, the power flow through the AC-link is calculated as

$$P = \frac{T_s}{12L_s} \frac{U'_{\rm dc2}(4U_{\rm dc1}^2 d_1 - 3U_{\rm dc1}^2 d_1^2 - U'^2_{\rm dc2})}{U_{\rm dc1}}. \tag{16}$$

In this mode, the converter power, passive duty cycle as well as PS all monotonically increase with the duty cycle increase. Interestingly, although the voltages are different, the derived current and power euqations are the same as those in CCM2.

TABLE III
TRANSFORMER PHASE CURRENT EQUATIONS FOR 3p-SAB CONVERTERS IN CCM3 UNDER HIGH DVCR CONDITIONS

Intervals	Transformer current i_L equations
$0 \sim t_1$	$i_1 - i_0 = \frac{2U_{dc1} + U'_{dc2}}{3L_s} T_s \Delta_d$
$t_1 \sim t_2$	$i_2 - i_1 = \frac{2U_{dc1} - U'_{dc2}}{3L_s} T_s (d_2 - \frac{1}{3})$
$t_2 \sim t_3$	$i_3 - i_2 = \frac{2U_{dc1} - 2U'_{dc2}}{3L_s} T_s (d_1 - d_2 - \Delta_d + \frac{1}{3})$
$t_3 \sim t_4$	$i_4 - i_3 = \frac{0 - 2U'_{dc2}}{3L_s} T_s (\frac{1}{3} - d_1)$
$t_4 \sim t_5$	$i_5 - i_4 = \frac{-U_{dc1} - 2U'_{dc2}}{3L_s} T_s \Delta_d$
$t_5 \sim t_6$	$i_6 - i_5 = \frac{-U_{dc1} - U'_{dc2}}{3L_s} T_s (d_2 - \frac{1}{3})$
$t_6 \sim t_7$	$i_7 - i_6 = \frac{-U_{dc1} + U'_{dc2}}{3L_s} T_s (d_1 - d_2 - \Delta_d + \frac{1}{3})$
$t_7 \sim t_8$	$i_8 - i_7 = \frac{0 + U'_{dc2}}{3L_s} T_s (\frac{1}{3} - d_1)$
$t_8 \sim t_9$	$i_9 - i_8 = \frac{2U_{dc1} + U'_{dc2}}{3L_s} T_s \Delta_d$
$t_9 \sim t_{10}$	$i_{10} - i_9 = \frac{-U_{dc1} + 2U'_{dc2}}{3L_s} T_s (d_2 - \frac{1}{3})$
$t_{10} \sim t_{11}$	$i_{11} - i_{10} = \frac{-U_{dc1} + U'_{dc2}}{3L_s} T_s (d_1 - d_2 - \Delta_d + \frac{1}{3})$
$t_{11} \sim T_s$	$i_0 - i_{11} = \frac{0 + U'_{dc2}}{3L_s} T_s (\frac{1}{3} - d_1)$

D. Discontinuous Current Mode

When the value of d_1 is in the range of $[0, \frac{U'_{dc2}}{3U_{dc1}}]$, the converter works in DCM as shown in Fig. 10. There are only nine intervals in this mode. All current equations are given in Table IV.

In this mode, since both d_1 and d_2 are smaller than 1/3, both voltages and transformer current have zero stages. Thus, Δ_d is 0 because no PS exists. The currents and d_2 can be solved and the results are given as (17)–(19)

$$i_1 = -2i_4 = -2i_7 = \frac{2T_s}{3L_s}\left(U_{\rm dc1} - U'_{\rm dc2}\right) d_1 \tag{17}$$

$$d_2 = \frac{U_{\rm dc1}}{U'_{\rm dc2}} d_1 \tag{18}$$

$$\Delta_d = 0. \tag{19}$$

Assume the converter is lossless, the power flow through the AC-link is calculated as

$$P = \frac{T_s}{L_s}\left(U_{\rm dc1} - U'_{\rm dc2}\right) U_{\rm dc1} d_1^2. \tag{20}$$

Obviously, the power quadratically grows with the increase of duty cycle.

V. OPERATIONAL PRINCIPLES OF 3p-SAB CONVERTERS UNDER LOW DVCR CONDITIONS

Four operating modes are also discovered when d_1 is in the range of [0, 0.5] under low DVCR conditions ($m < 1/2$). There are three CCMs and one DCCMs as well. Similarly, 12 intervals can be found in the continuous modes and 9 intervals exist in the discontinuous mode. However, except the first CCM, the other modes have the same equations and solutions as the corresponding high DVCR scenarios, making the analysis simplified.

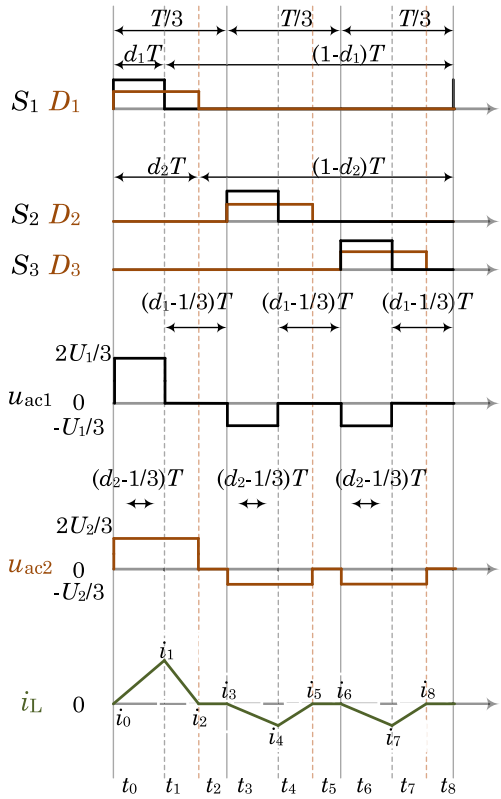

Fig. 10. Waveforms of 3p-SAB converters in DCM under high DVCR conditions.

TABLE IV
TRANSFORMER PHASE CURRENT EQUATIONS FOR 3p-SAB CONVERTERS IN DCM UNDER HIGH DVCR CONDITIONS

Intervals	Transformer current i_L equations
$0 \sim t_1$	$i_1 - i_0 = \frac{2U_{dc1} - 2U'_{dc2}}{3L_s} T_s d_1$
$t_1 \sim t_2$	$i_2 - i_1 = \frac{0 - U'_{dc2}}{3L_s} T_s (d_2 - d_1)$
$t_2 \sim t_3$	$i_3 - i_2 = \frac{0 - 0}{3L_s} T_s (\frac{1}{3} - d_2)$
$t_3 \sim t_4$	$i_4 - i_3 = \frac{-U_{dc1} + U'_{dc2}}{3L_s} T_s d_1$
$t_4 \sim t_5$	$i_5 - i_4 = \frac{0 + U'_{dc2}}{3L_s} T_s (d_2 - d_1)$
$t_5 \sim t_6$	$i_6 - i_5 = \frac{0 - 0}{3L_s} T_s (\frac{1}{3} - d_2)$
$t_6 \sim t_7$	$i_7 - i_6 = \frac{-U_{dc1} + U'_{dc2}}{3L_s} T_s d_1$
$t_7 \sim t_8$	$i_8 - i_7 = \frac{0 + U'_{dc2}}{3L_s} T_s (d_2 - d_1)$
$t_8 \sim T_s$	$i_0 - i_8 = \frac{0 - 0}{3L_s} T_s (\frac{1}{3} - d_2)$

A. Continuous Current Mode 1

When the value of d_1 is large and in the range of $[\frac{U_{\rm dc1} + U'_{\rm dc2}}{3U_{\rm dc1}}, \frac{1}{2}]$, the converter works in low voltage Continuous Current Mode 1 (CCM1) as shown in Fig. 11. There are 12 intervals and in each interval, the slope of the linear phase current

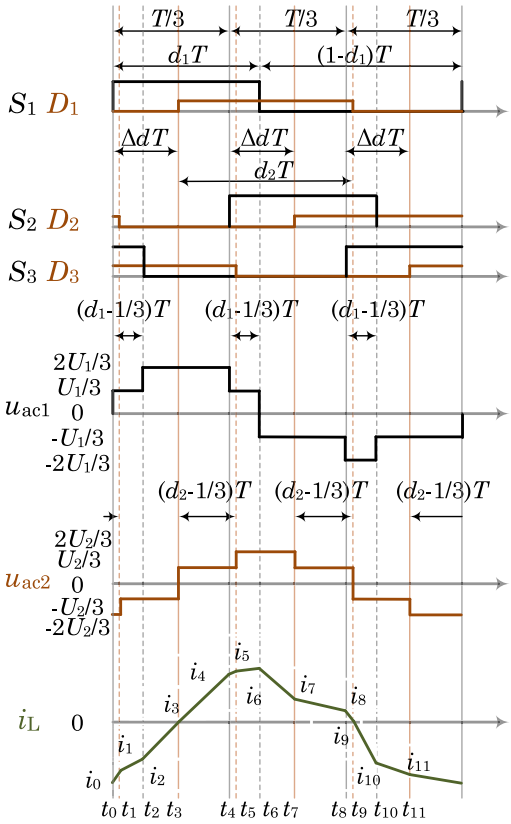

Fig. 11. Waveforms of 3p-SAB converters in CCM1 under low DVCR conditions.

equation is determined by $u_{\rm ac1}$ and $u_{\rm ac2}$. All current equations are given in Table V.

Since the three phases are symmetric, the last four currents $i_8 \sim i_{11}$ can also be found by the symmetric current conditions in (1).

At t_3 and t_9, the transformer current crosses zero so the zero current conditions are

$$i_3 = 0, \quad i_9 = 0. \tag{21}$$

The other six currents, two switch state variables d_2 and Δ_d need to be solved, and the first eight equations in Table V are independent. As a result, the solved results are given as (22)–(24). For the sake of brevity, only i_0 is shown here and the rest currents can be derived using Table V.

$$i_0 = -\frac{T_s}{18L_s}\frac{2U_{\rm dc1}^2 + 6U_{\rm dc1}U'_{\rm dc2}d_1 - 3U_{\rm dc1}U'_{\rm dc2} - 2U'^2_{\rm dc2}}{U_{\rm dc1}} \tag{22}$$

$$d_2 = \frac{1}{2} \tag{23}$$

$$\Delta_d = \frac{3U_{\rm dc1}d_1 - U'_{\rm dc2}}{6U_{\rm dc1}}. \tag{24}$$

TABLE V
TRANSFORMER PHASE CURRENT EQUATIONS FOR 3p-SAB CONVERTERS IN CCM1 UNDER LOW DVCR CONDITIONS

Intervals	Transformer current i_L equations
$0 \sim t_1$	$i_1 - i_0 = \frac{U_{dc1} + 2U'_{dc2}}{3L_s}T_s(\Delta_d - \frac{2}{3} + d_2)$
$t_1 \sim t_2$	$i_2 - i_1 = \frac{U_{dc1} + U'_{dc2}}{3L_s}T_s(\frac{1}{3} - \Delta_d + d_1 - d_2)$
$t_2 \sim t_3$	$i_3 - i_2 = \frac{2U_{dc1} + U'_{dc2}}{3L_s}T_s(\Delta_d - d_1 + \frac{1}{3})$
$t_3 \sim t_4$	$i_4 - i_3 = \frac{2U_{dc1} - U'_{dc2}}{3L_s}T_s(\frac{1}{3} - \Delta_d)$
$t_4 \sim t_5$	$i_5 - i_4 = \frac{U_{dc1} - U'_{dc2}}{3L_s}T_s(\Delta_d - \frac{2}{3} + d_2)$
$t_5 \sim t_6$	$i_6 - i_5 = \frac{U_{dc1} - 2U'_{dc2}}{3L_s}T_s(\frac{1}{3} - \Delta_d + d_1 - d_2)$
$t_6 \sim t_7$	$i_7 - i_6 = \frac{-U_{dc1} - 2U'_{dc2}}{3L_s}T_s(\Delta_d - d_1 + \frac{1}{3})$
$t_7 \sim t_8$	$i_8 - i_7 = \frac{-U_{dc1} - U'_{dc2}}{3L_s}T_s(\frac{1}{3} - \Delta_d)$
$t_8 \sim t_9$	$i_9 - i_8 = \frac{-2U_{dc1} - U'_{dc2}}{3L_s}T_s(\Delta_d - \frac{2}{3} + d_2)$
$t_9 \sim t_{10}$	$i_{10} - i_9 = \frac{-2U_{dc1} + U'_{dc2}}{3L_s}T_s(\frac{1}{3} - \Delta_d + d_1 - d_2)$
$t_{10} \sim t_{11}$	$i_{11} - i_{10} = \frac{-U_{dc1} + U'_{dc2}}{3L_s}T_s(\Delta_d - d_1 + \frac{1}{3})$
$t_{11} \sim T_s$	$i_0 - i_{11} = \frac{-U_{dc1} + 2U'_{dc2}}{3L_s}T_s(\frac{1}{3} - \Delta_d)$

Assume the converter is lossless, the power flow through the ac-link is calculated as

$$P = \frac{T_s}{36L_s}\frac{U'_{\rm dc2}(18U_{\rm dc1}^2 d_1 - 18U_{\rm dc1}^2 d_1^2 - U_{\rm dc1}^2 - 2U'^2_{\rm dc2})}{U_{\rm dc1}}. \tag{25}$$

Interestingly, in this mode even the duty cycle is changed, the secondary side duty cycle d_2 is not changed. The PS and power flow decreases with the decrease of d_1.

B. Continuous Current Mode 2

When the value of d_1 is in the range of $[\frac{1}{3}, \frac{U_{\rm dc1}+U'_{\rm dc2}}{3U_{\rm dc1}}]$, the converter works in CCM2 as shown in Fig. 12. There are 12 intervals and it can be found although the PS is larger, the current equations are the same as CCM2 under the high DVCR scenario, which are given in Table II.

The symmetric conditions and zero-current conditions are also identical to those in the high DVCR scenario, so the currents, d_2 and Δ_d can be calculated as

$$i_0 = -\frac{T_s}{18L_s}\frac{2U_{\rm dc1}^2 + 3U_{\rm dc1}U'_{\rm dc2}d_1 - 2U_{\rm dc1}U'_{\rm dc2} - U'^2_{\rm dc2}}{U_{\rm dc1}} \tag{26}$$

$$d_2 = \frac{3U_{\rm dc1}d_1 - U'_{\rm dc2} + 2U_{\rm dc1}}{6U_{\rm dc1}} \tag{27}$$

$$\Delta_d = \frac{3U_{\rm dc1}d_1 - U'_{\rm dc2}}{6U_{\rm dc1}}. \tag{28}$$

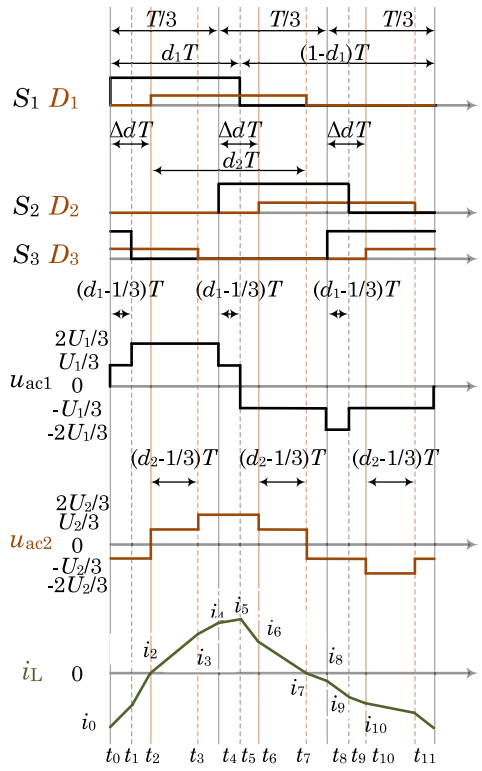

Fig. 12. Waveforms of 3p-SAB converters in CCM2 under low DVCR conditions.

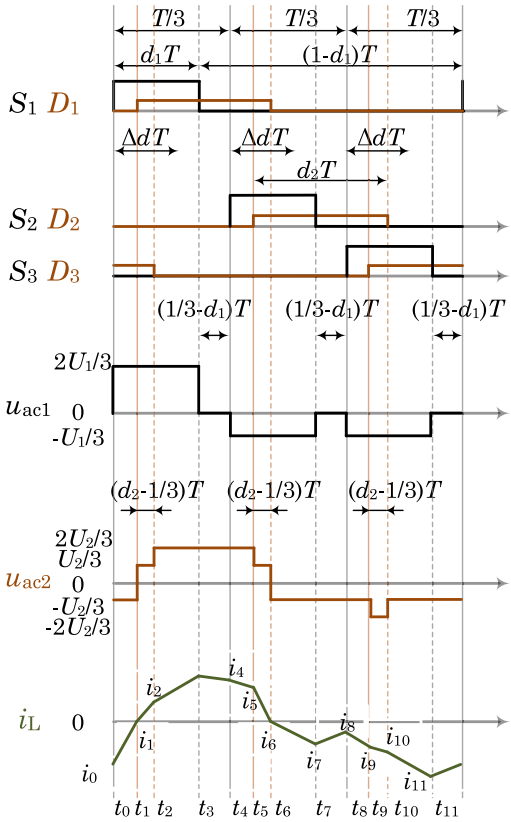

Fig. 13. Waveforms of 3p-SAB converters in CCM3 under low DVCR conditions.

Assume the converter is lossless, the power flow through the ac-link is calculated as

$$P = \frac{T_s}{12L_s}\frac{U'_{\rm dc2}(4U_{\rm dc1}^2 d_1 - 3U_{\rm dc1}^2 d_1^2 - U'^2_{\rm dc2})}{U_{\rm dc1}}. \tag{29}$$

In this mode, the power increases monotonically with the increase of d_1.

C. Continuous Current Mode 3

When the value of d_1 is in the range of $[\frac{U_{\rm dc2}}{3U_{\rm dc1}}, \frac{1}{3}]$, the converter works in CCM3 as shown in Fig. 13. Also, although the PS is larger, the current equations are the same as CCM3 under the high DVCR scenario, which are given in Table III.

The symmetric conditions and zero-current conditions are also identical to those under the high DVCR scenario, so the variables can be calculated as

$$i_0 = -\frac{T_s}{18L_s}\frac{(2U_{\rm dc1} + U'_{\rm dc2})(3U_{\rm dc1}d_1 - U'_{\rm dc2})}{U_{\rm dc1}} \tag{30}$$

$$d_2 = \frac{3U_{\rm dc1}d_1 - U'_{\rm dc2} + 2U_{\rm dc1}}{6U_{\rm dc1}} \tag{31}$$

$$\Delta_d = \frac{3U_{\rm dc1}d_1 - U'_{\rm dc2}}{6U_{\rm dc1}}. \tag{32}$$

Assume the converter is lossless, the power flow through the ac-link is calculated as

$$P = \frac{T_s}{12L_s}\frac{U'_{\rm dc2}(4U_{\rm dc1}^2 d_1 - 3U_{\rm dc1}^2 d_1^2 - U'^2_{\rm dc2})}{U_{\rm dc1}}. \tag{33}$$

Interestingly, although the voltages are different, the derived current and power equations are the same as those in CCM2.

D. Discontinuous Current Mode

When the value of d_1 is in the range of $[0, \frac{U'_{\rm dc2}}{3U_{\rm dc1}}]$, the converter works in discontinuous current mode (DCM) as shown in Fig. 14. There are only nine intervals in this mode. All current equations are the same as DCM under the high DVCR condition, which are given in Table IV.

In this mode, the derivations of currents and power flow follow the same process described in Section III.D. The results are given as follows:

$$i_1 = -2i_4 = -2i_7 = \frac{2T_s}{3L_s}(U_{\rm dc1} - U'_{\rm dc2})\, d_1 \tag{34}$$

$$d_2 = \frac{U_{\rm dc1}}{U'_{\rm dc2}} d_1 \tag{35}$$

$$\Delta_d = 0. \tag{36}$$

Assume the converter is lossless, the power flow through the ac-link is calculated as

$$P = \frac{T_s}{L_s}(U_{\rm dc1} - U'_{\rm dc2})\, U_{\rm dc1} d_1^2. \tag{37}$$

Also, the power quadratically grows with the increase of duty cycle.

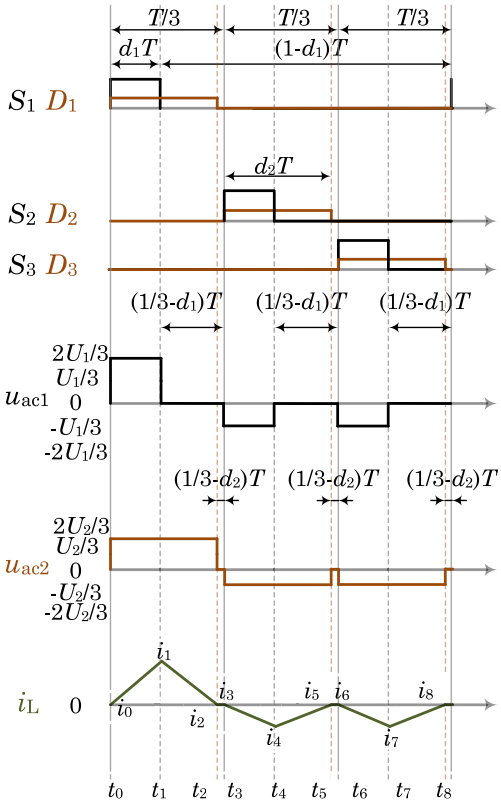

Fig. 14. Waveforms of 3p-SAB converters in DCM under low DVCR conditions.

VI. Performance Evaluation and Comparison

After completing the theoretical analyses in Sections III and IV, the performances of 3p-SAB converters under different duty cycles and DVCRs can be evaluated and compared. The evaluation and comparison endeavor to provide insights into the impacts of varying duty cycles and different DVCRs on the power flow, the transformer and the input and output capacitors, so that the converter design could have those as references. For the sake of comparison, the power and current are normalized. Ideally, the maximum power should be used as the base value. However, the maximum power expression is very complex, and therefore, in order to normalize the maximum power close to 1 p.u., $P_0 = T_s U_{\rm dc1}^2/25L_s$ is chosen instead. Accordingly, the current base values used on both sides are defined as follows:

$$\begin{aligned} P_0 &= \frac{T_s U_{\rm dc1}^2}{25L_s} \\ I_{\rm dc1} &= \frac{T_s U_{\rm dc1}}{25L_s} \\ I_{\rm dc2} &= \frac{T_s U_{\rm dc1}^2}{25L_s U'_{\rm dc2}} = \frac{T_s U_{\rm dc1}^2}{25L_s m}. \end{aligned} \tag{38}$$

A. Power Flow Analysis

The power flow expressions when the DVCR is high ($m = U'_{\rm dc2}/U_{\rm dc1} > 1/2$) are given in (6), (11), (16), and (20). The normalized converter power flow P/P_0 is a function with respect to m and active bridge duty cycle d_1. P/P_0 under high DVCR conditions is summarized here as follows:

$$P/P_0 = \begin{cases} 25(1-m)d_1^2 & 0 \le d_1 \le \dfrac{m}{3} \\ \dfrac{25}{12}m\left(4d_1 - 3d_1^2 - m^2\right) & \dfrac{m}{3} \le d_1 \le \dfrac{1}{3} \\ \dfrac{25}{12}m\left(4d_1 - 3d_1^2 - m^2\right) & \dfrac{1}{3} \le d_1 \le \dfrac{2-m}{3} \\ \dfrac{25}{9}m\left(1 - m^2\right) & \dfrac{2-m}{3} \le d_1 \le \dfrac{1}{2}. \end{cases} \tag{39}$$

The power flow expressions of the low DVCR ($m \le 1/2$) are shown in (25), (29), (33), and (37). P/P_0 under low DVCR conditions is summarized here as follows:

$$P/P_0 = \begin{cases} 25(1-m)d_1^2 & 0 \le d_1 \le \dfrac{m}{3} \\ \dfrac{25}{12}m\left(4d_1 - 3d_1^2 - m^2\right) & \dfrac{m}{3} \le d_1 \le \dfrac{1}{3} \\ \dfrac{25}{12}m\left(4d_1 - 3d_1^2 - m^2\right) & \dfrac{1}{3} \le d_1 \le \dfrac{m+1}{3} \\ \dfrac{25}{36}m\left(18d_1 - 18d_1^2 - 1 - 2m^2\right) & \dfrac{m+1}{3} \le d_1 \le \dfrac{1}{2}. \end{cases} \tag{40}$$

If d_1 is in the range of $[\frac{2-m}{3}, \frac{1}{2}]$ and $m \ge 0.5$, the PS is not changed and the power flow is constant. Therefore, in order to control the converter power under high DVCR conditions, the duty cycle must be less than $\frac{2-m}{3}$. It means that the converter would hardly work in the basic operation when the duty cycle $d_1 = 0.5$. In order to depict the power flow better, the normalized three-dimension (3-D) power flow with respect to d_1 and m is demonstrated in Fig. 15.

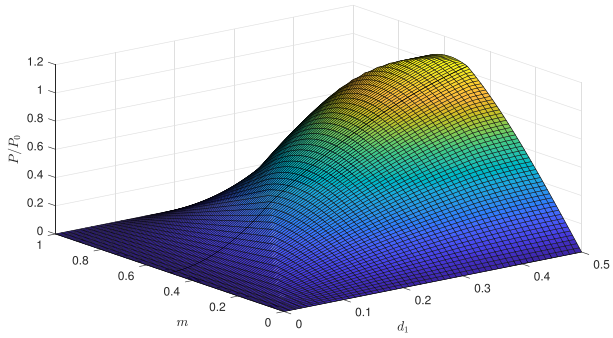

Fig. 15. 3-D power flow of 3p-SAB converters versus duty cycle and DVCR.

Several interesting conclusions can be found from the 3-D power flow diagram. Given constant input and output voltage ratio m, the converter power will increase monotonically with d in the range of [0, 0.5]. Therefore, the maximum power is always achieved when $d_1 = 0.5$, whatever m is. When $d_1 = 0.5$, the converter power has a global maximum at $m = \sqrt{3}/3$, given fixed leakage inductance, switching frequency, and input dc voltage.

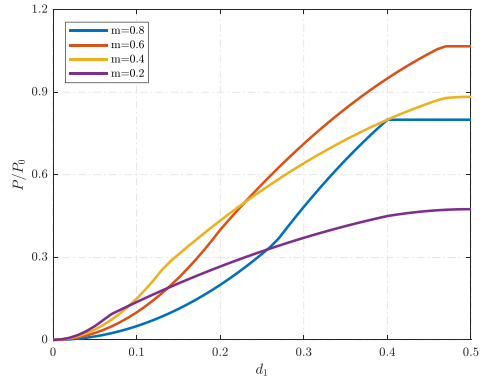

Fig. 16. 2-D power flow of 3p-SAB converters versus duty cycle.

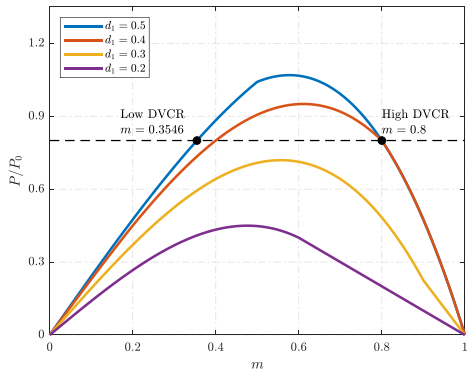

Fig. 17. 2-D power flow of 3p-SAB converters versus DVCR.

When the duty cycle is fixed, the converter power changes with the change of m. The converter power increases with m before m reaches the argument of the maximum power. After the argument, the converter power decreases with m. This implies that if the duty cycle is uncontrolled and m is large, the converter power will actually increase when m decreases. The decrease in m normally means a grid voltage sag, and this conclusion shows that the converter is able to provide support in this condition.

The 2-D power flow diagrams versus d_1 and m are presented in Figs. 16 and 17, respectively. From Fig. 16, it is shown again that the converter power will increase monotonically with d_1, under each DVCR condition. Despite different d_1, there is a maximum power with the change of m in Fig. 17.

For a further comparison, two different DVCR values: $m = 0.8$ and $m = 0.3546$ are chosen to represent the high DVCR and low DVCR condition in the following analysis. The converter has the same maximum power under these two conditions, as shown in Fig. 17.

B. Impact on Switches and AC-Link MV Transformers

The transformer current and transformer voltage have significant impacts on the converter switching losses, transformer core and winding losses, and current stress. In 3p-SAB converters, the common harmonics are in the order of multiples of three, which are eliminated in the ac transformer current and voltage waveforms, as shown in Figs. 5 and 6.

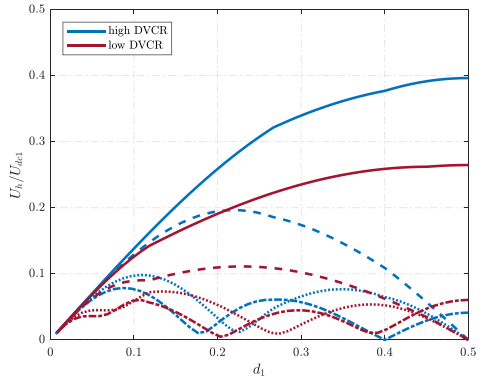

Fig. 18. Transformer rms voltage harmonics of 3p-SAB converters under high and low DVCR condition (solid line: fundamental frequency; dashed line: second harmonics; dotted line: fourth harmonics; dashed-dotted line: fifth harmonics).

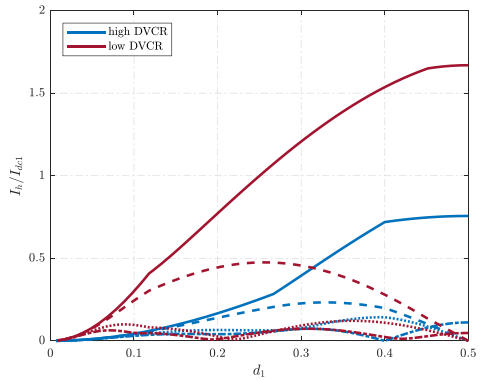

Fig. 19. Transformer rms current harmonics of 3p-SAB converters under high and low DVCR condition (solid line: fundamental frequency; dashed line: second harmonics; dotted line: fourth harmonics; dashed-dotted line: fifth harmonics).

The rms values of voltage $e_m = (u_{\mathrm{ac1}} + u_{\mathrm{ac2}})/2$ and current i_L are used to calculate the transformer magnetic core losses and winding losses, respectively [29]. It is necessary to analyze them under different duty cycles, not only under the 50% duty cycle. The rms values of e_m and i_L are presented in Figs. 18 and 19.

It can be seen that the fundamental component is the largest among all harmonics. The fundamental components in e_m and i_L both reach the maximum at $d_1 = 0.5$, but the rest harmonics fluctuate with the change of duty cycle. In terms of e_m, under the high DVCR condition it is nearly 40% larger than that of the low DVCR condition. However, the low DVCR shows significantly larger harmonic currents, around two times more than those under the high DVCR.

Note that the harmonic currents not only increase the transformer winding losses, but also increase the converter conductive losses. Hence, the resulting overall converter efficiency should have a strong correlation with the rms values of i_L. Therefore, it is suggested to design 3p-SAB converters under high DVCRs with higher secondary dc voltages. The efficiency advantage is verified by the experimental results in the next section.

The transformer utilization factor (TUF) used in [28] and, [31] is analyzed here as well. It is expressed as: TUF $= \frac{P}{S}$, where P is the active power and S is the apparent power of the transformer.

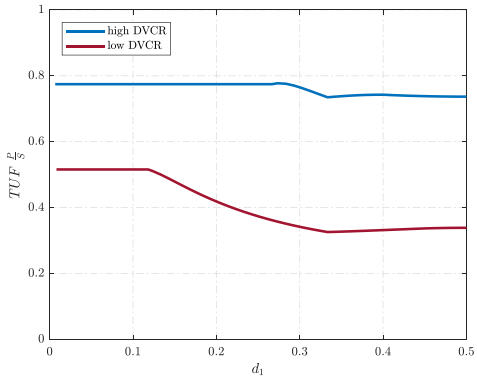

Fig. 20. TUF of 3p-SAB converters under high and low DVCR condition.

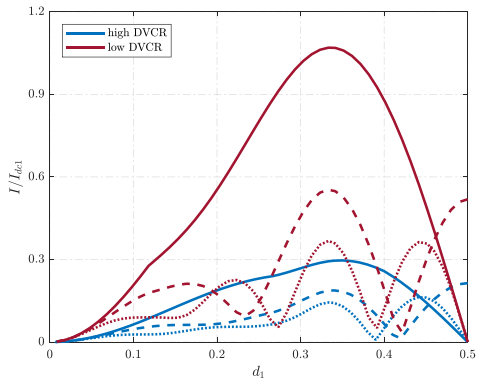

Fig. 21. Input rms current harmonics of 3p-SAB converters under high and low DVCR condition (solid line: third harmonics; dashed line: sixth harmonics; dotted line: ninth harmonics).

It reflects the utilization percentage of the transformer. The TUF results are presented in Fig. 20. It can be seen that the converter has a larger TUF under the high DVCR condition within the whole operating range.

The zero-voltage-switching turn-ON is always achieved for 3p-SAB converters whatever d_1 and m are, while on the contrary the turn-OFF is always hard-switching. Therefore, it is also crucial to investigate the turn-OFF current performance. The peak current represents the converter current stress and thus also requires attention. The analytical results of peak current and turn-OFF current are presented and compared with experimental results in the next section.

C. Impact on Input and Output Filters

Only the dc component and harmonics with the order of multiples of three exist in the dc input and output currents. In fact, the dc currents contain substantial harmonics, requiring larger capacitors on both sides. Figs. 21 and 22 depict the rms values of input and current harmonics. The input and output current are normalized on the currents given in (38).

The high DVCR and the low DVCR condition both have larger normalized harmonics in the input current than in the output current. The dominant components are the third harmonic for both the input and output current. The third harmonic current

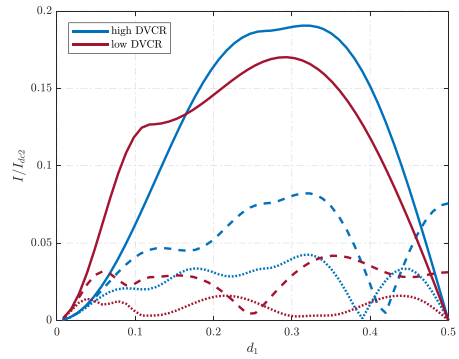

Fig. 22. Output rms current harmonics of 3p-SAB converters under high and low DVCR condition (solid line: third harmonics; dashed line: sixth harmonics; dotted line: ninth harmonics).

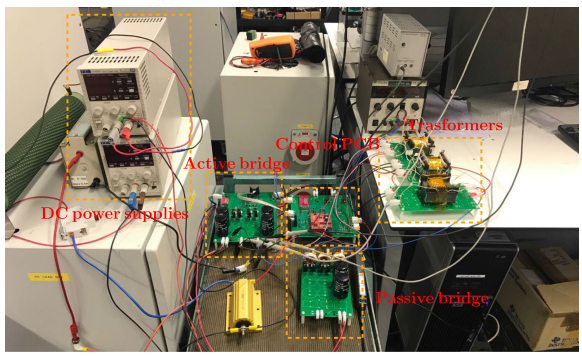

Fig. 23. Experimental 3p-SAB converter prototype.

TABLE VI
EXPERIMENTAL PROTOTYPE PARAMETERS

Parameter	Value
U_{dc1}, U_{dc2}	60V, 48V or 21.3V
N	1 : 1
L_s	0.56mH
f_s	5kHz
C_{dc1}, C_{dc2}	3.3mF

hits its maximum when d_1 is in the range of [0.3, 0.4] for both DVCR conditions in the input current. Although it has a flat high value range in the output current, the normalized value (smaller than 0.2) is still much smaller than the maximum input harmonic current (around 1.2). Furthermore, the high DVCR condition features substantially lower input current harmonics compared with the counterpart, and slightly higher output current harmonics. Therefore, for the low DVCR condition, the input capacitor should be designed significantly larger.

VII. EXPERIMENTAL RESULTS

In order to validate the analytical expressions derived, an experiment prototype has been developed to test the performances, as shown in Fig. 23. The parameters of the prototype are given in Table VI. In this experiment, $U_{\rm dc2} = 48$ V represents the high DVCR condition, and $U_{\rm dc2} = 21.3$ V represents the low DVCR case.

Figs. 24 and 25 show the waveforms of bridge middle point voltages (from bridge middle point to ground) $u_{\rm AO}$ and $u_{\rm ao}$ and

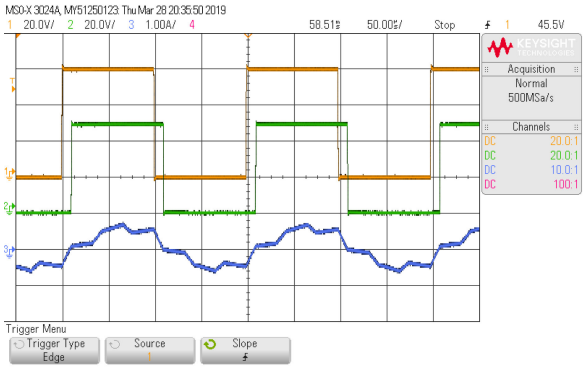

(a)

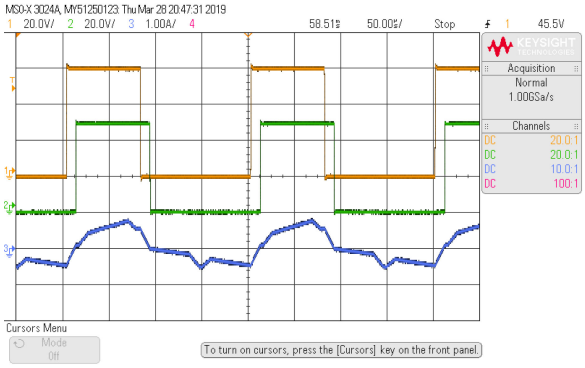

(b)

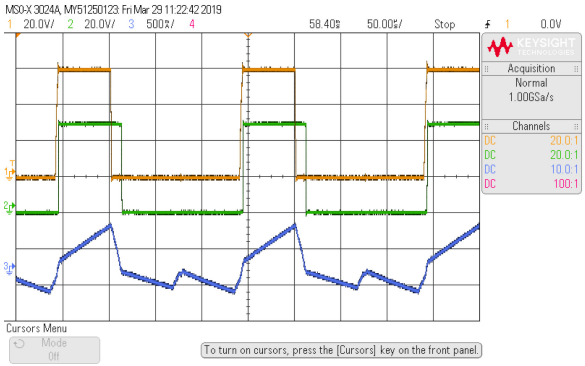

(c)

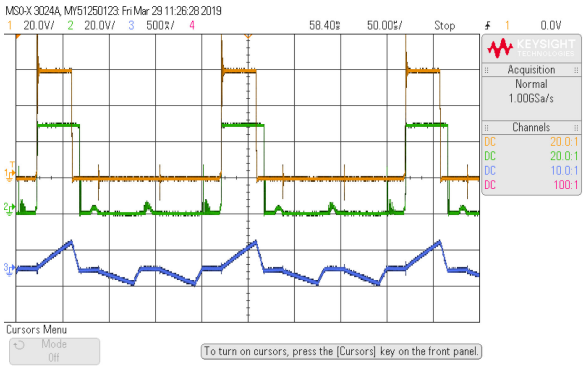

(d)

Fig. 24. Experimental bridge middle point voltages and transformer phase current of the 3p-SAB converter under high DVCR condition. (a) Continuous Current Mode 1 ($d_1 = 0.5$). (b) Continuous Current Mode 2 ($d_1 = 0.4$). (c) Continuous Current Mode 3 ($d_1 = 0.3$). (d) Discontinuous Current Mode ($d_1 = 0.2$).

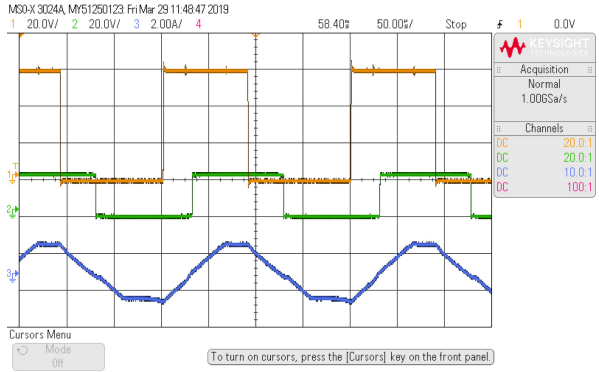

(a)

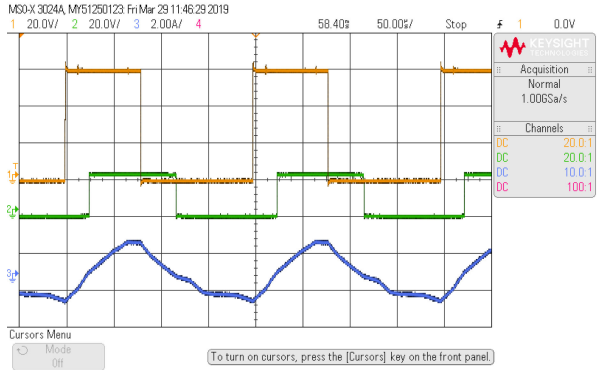

(b)

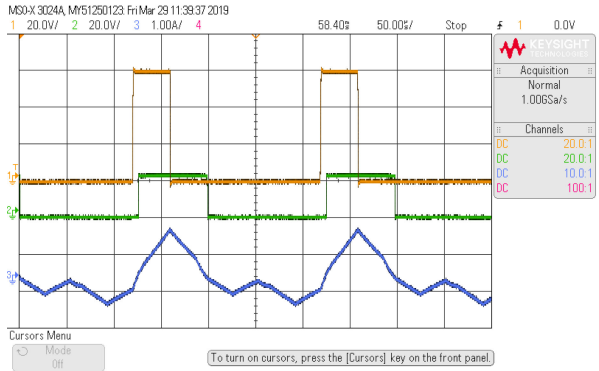

(c)

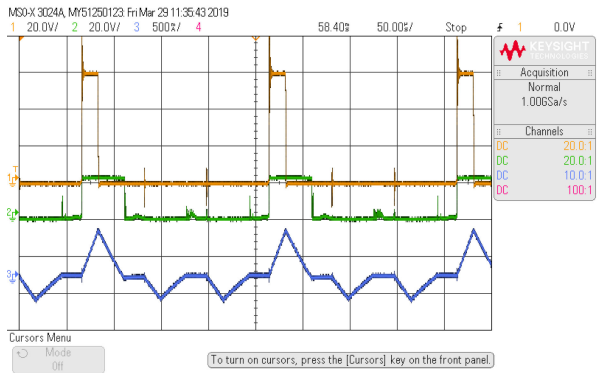

(d)

Fig. 25. Experimental bridge middle point voltages and transformer phase current of the 3p-SAB converter under low DVCR condition. (a) CCM 1 ($d_1 = 0.45$). (b) CCM 2 ($d_1 = 0.4$). (c) CCM 3 ($d_1 = 0.2$). (d) DCM ($d_1 = 0.1$).

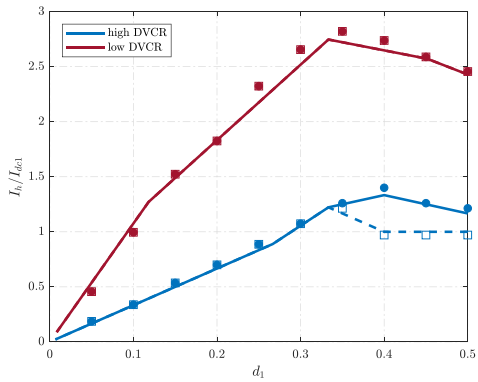

Fig. 26. Analytical and experimental peak current and turn-OFF current of the 3p-SAB converter under high and low DVCR condition (solid line: analytical peak current; dashed line: analytical turn-OFF current; square marker: experimental peak current; round marker: experimental turn-OFF current).

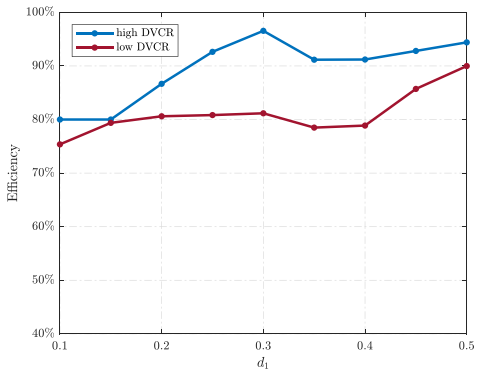

Fig. 27. Prototype converter efficiency versus active bridge duty cycle.

transformer current i_L under the high DVCR and low DVCR condition. The current shapes can be seen very closely matching the theoretical waveforms shown in Sections IV and V.

As mentioned in Section VI, the converter turn-OFF and peak current are also measured and are compared with the theoretical results here. Fig. 26 shows that the measured currents closely match the analytical normalized currents, verifying that the high DVCR condition shows much smaller turn-OFF currents and peak currents. Moreover, the turn-OFF current is the same as the peak current under the low DVCR condition ($m = 0.3546$), but under the high DVCR condition ($m = 0.8$) when $d_1 > 1/3$, the turn-OFf current is smaller than the peak current. Note that since the low DVCR turn-OFF currents are almost two times those under the high DVCR, significant switching losses should be seen under the low DVCR condition, given the same semiconductor devices. This conclusion also suggests that the converter should operate in high DVCR conditions.

As discussed before, the overall converter efficiency can be affected by the transformer current, transformer voltage, and active bridge turn-OFF current. Although the low DVCR condition has a slightly better transformer voltage, it makes the transformer harmonic currents and turn-OFF current significantly larger. Therefore, a higher efficiency should be expected under the high DVCR condition.

Fig. 27 shows the experimental efficiency curves obtained via measuring the two side dc power. It proves that the high DVCR condition outperforms the opposite in terms of efficiency in the whole duty cycle range. It is also worth noticing that the efficiency achieves a maximum around $d_1 = 0.3$ and then drops slightly; however, it then interestingly increases if the duty cycle further increases. One possible explanation for this trend is that the turn-OFF current starts to decrease from $1/3$ (see Fig. 26), which results in reduced switching losses and perhaps increases the efficiency.

VIII. Discussions and Conclusion

SAB converters are regarded as a potential option for MV dc/dc converters. When the voltage level is to be stepped up to medium level (e.g., 5–50 kV), semiconductor voltage blocking capability becomes the main concern, especially at the high-voltage side. If the multilevel concept is not used, the serial connection of semiconductors is the only viable option. However, the semiconductor voltage sharing problem arises from this option. Compared with actively controlled semiconductors, diodes can be easily connected in series and effective voltage sharing is easier to implement. SAB converters can be assembled with series-connected diode-based passive bridges so that very high secondary voltage rating can be achieved, which makes them suitable candidates for high step-up MV dc/dc conversion applications, such as dc wind farms.

This article presents the identified eight operating modes under different voltage and duty cycle conditions for 3p-SAB dc/dc converters. Detailed derivations of the converter currents, duty cycles, and power flow are provided. The complicated relationships among the active bridge duty cycle and the secondary duty cycle, the PS angle and the converter power flow are formulated.

The evaluation and comparison between the high and low DVCR condition are conducted, through analyzing the transformer ac current and voltage, converter peak current and turn-OFF current, and input and output dc currents. The results indicate that the high conversion ratio condition substantially outperforms the low conversion ratio in terms of transformer rms current, switching losses, and total transformer utilization ratio. Moreover, the high conversion ratio condition features much fewer input current harmonics, resulting in a smaller input capacitor design. Therefore, the converter should be designed and operate in high DVCR conditions. However, if the secondary side has a fault and the secondary dc voltage becomes extremely low, the converter is still be able to deliver some fault current. However, the amount of power that can be delivered should be very small, since the reactive power is large under extremely low DVCR conditions. The converter peak current should be carefully monitored when the converter tries to deliver faulty current.

Finally, a scale-down experimental prototype is built to verify the findings. The measured results justify that the converter has the same current shapes as those in theoretical analysis. The high DVCR condition outperforms the low DVCR condition in terms of turn-OFF current, peak current, and total efficiency.

REFERENCES

[1] S. Inoue and H. Akagi, "A bidirectional DC–DC converter for an energy storage system with galvanic isolation," *IEEE Trans. Power Electron.*, vol. 22, no. 6, pp. 2299–2306, Nov. 2007.

[2] H. Bai and C. Mi, "Eliminate reactive power and increase system efficiency of isolated bidirectional dual-active-bridge DC–DC converters using novel dual-phase-shift control," *IEEE Trans. Power Electron.*, vol. 23, no. 6, pp. 2905–2914, Nov. 2008.

[3] B. Zhao, Q. Song, W. Liu, and Y. Sun, "Overview of dual-active-bridge isolated bidirectional DC–DC converter for high-frequency-link power-conversion system," *IEEE Trans. Power Electron.*, vol. 29, no. 8, pp. 4091–4106, Aug. 2013.

[4] N. M. L. Tan, T. Abe, and H. Akagi, "Design and performance of a bidirectional isolated DC–DC converter for a battery energy storage system," *IEEE Trans. Power Electron.*, vol. 27, no. 3, pp. 1237–1248, Mar. 2011.

[5] F. Z. Peng, H. Li, G.-J. Su, and J. S. Lawler, "A new ZVS bidirectional DC–DC converter for fuel cell and battery application," *IEEE Trans. Power Electron.*, vol. 19, no. 1, pp. 54–65, 2004.

[6] Y. Du, X. Zhou, S. Bai, S. Lukic, and A. Huang, "Review of non-isolated bi-directional DC–DC converters for plug-in hybrid electric vehicle charge station application at municipal parking decks," in *Proc. 25th Annu. IEEE Appl. Power Electron. Conf. Expo.*, 2010, pp. 1145–1151.

[7] R. W. De Doncker, D. M. Divan, and M. H. Kheraluwala, "A three-phase soft-switched high power density DC/DC converter for high power applications," in *Proc. Conf. Rec. IEEE Ind. Appl. Soc. Annu. Meeting*, 1988, pp. 796–805.

[8] H. Qin and J. W. Kimball, "Generalized average modeling of dual active bridge DC–DC converter," *IEEE Trans. Power Electron.*, vol. 27, no. 4, pp. 2078–2084, Apr. 2012.

[9] F. Krismer and J. W. Kolar, "Efficiency-optimized high-current dual active bridge converter for automotive applications," *IEEE Trans. Ind. Electron.*, vol. 59, no. 7, pp. 2745–2760, Jul. 2012.

[10] D. Segaran, D. G. Holmes, and B. P. McGrath, "Enhanced load step response for a bidirectional DC–DC converter," *IEEE Trans. Power Electron.*, vol. 28, no. 1, pp. 371–379, Jan. 2013.

[11] N. Soltau, H. Stagge, R. De Doncker, and O. Apeldoorn, "Development and demonstration of a medium-voltage high-power DC–DC converter for DC distribution systems," in *Proc. IEEE 5th Int. Symp. Power Electron. Distrib. Gener. Syst.*, Jun. 2014, pp. 1–8.

[12] S. P. Engel, N. Soltau, H. Stagge, and R. W. De Doncker, "Dynamic and balanced control of three-phase high-power dual-active bridge DC–DC converters in DC-grid applications," *IEEE Trans. Power Electron.*, vol. 28, no. 4, pp. 1880–1889, Apr. 2013.

[13] J. Huang, Z. Li, L. Shi, Y. Wang, and J. Zhu, "Optimized modulation and dynamic control of a three-phase dual active bridge converter with variable duty cycles," *IEEE Trans. Power Electron.*, vol. 34, no. 3, pp. 2856–2873, Mar. 2019.

[14] K. Park and Z. Chen, "Control and dynamic analysis of a parallel-connected single active bridge DC–DC converter for DC-grid wind farm application," *IET Power Electron.*, vol. 8, no. 5, pp. 665–671, May 2015. [Online]. Available: http://digital-library.theiet.org/content/journals/10.1049/iet-pel.2014.0420

[15] C. Fontana, M. Forato, K. Kumar, M. T. Outeiro, M. Bertoluzzo, and G. Buja, "Soft-switching capabilities of SAB vs. DAB converters," in *Proc. 41st Annu. Conf. IEEE Ind. Electron. Soc.*, 2015, pp. 3485–3490.

[16] G. D. Demetriades, "On small-signal analysis and control of the single- and the dual-active bridge topologies," doctoral dissertation, Roy. Inst. Technol. Dept. Elect. Eng. Elect. Mach. Power Electron, Stockholm, 2005.

[17] J. Jacobs, M. Thommes, and R. De Doncker, "A transformer comparison for three-phase single active bridges," *Eur. Conf. Power Electron. Appl.*, 2005, p. 10.

[18] A. Garcia-Bediaga, I. Villar, I. Etxeberria-Otadui, P. Barrade, and A. Rufer, "Comparison of multi-phase SAB converters vs. multi-phase SRC converters," in *Proc. IEEE Energy Convers. Congr. Expo.*, 2013, pp. 5448–5455.

[19] C. Sommer, A. Mertens, I. Larrazabal, and I. Kortazar, "Analytical investigation of the three-phase single active bridge for offshore applications," in *Proc. 18th Eur. Conf. Power Electron. Appl.*, 2016, pp. 1–10.

[20] C. Meyer, M. Hoing, A. Peterson, and R. W. De Doncker, "Control and design of DC-grids for offshore wind farms," in *Proc. Conf. Rec. IEEE Ind. Appl. Conf. 41st IAS Annu. Meeting*, 2006, vol. 3, 2006, pp. 1148–1154.

[21] J. Yang, J. E. Fletcher, and J. O'Reilly, "Multiterminal DC wind farm collection grid internal fault analysis and protection design," *IEEE Trans. Power Del.*, vol. 25, no. 4, pp. 2308–2318, Oct. 2010.

[22] D. Xu, C. Zhao, and H. Fan, "A PWM plus phase-shift control bidirectional DC–DC converter," *IEEE Trans. Power Electron.*, vol. 19, no. 3, pp. 666–675, May 2004.

[23] B. Zhao, Q. Yu, and W. Sun, "Extended-phase-shift control of isolated bidirectional DC–DC converter for power distribution in microgrid," *IEEE Trans. Power Electron.*, vol. 27, no. 11, pp. 4667–4680, Nov. 2012.

[24] F. Krismer and J. W. Kolar, "Accurate small-signal model for the digital control of an automotive bidirectional dual active bridge," *IEEE Trans. Power Electron.*, vol. 24, no. 12, pp. 2756–2768, Dec. 2009.

[25] L. Max and S. Lundberg, "System efficiency of a DC/DC converter-based wind farm," *Wind Energy, Int. J. Prog. Appl. Wind Power Convers. Technol.*, vol. 11, no. 1, pp. 109–120, 2008.

[26] Y. Cui, D. Wang, and A. Emadi, "Three-phase dual active bridge converter design considerations," in *Proc. 43rd Annu. Conf. IEEE Ind. Electron. Soc.*, 2017, pp. 4696–4701.

[27] A. Garcia-Bediaga, I. Villar, A. Rujas, I. Etxeberria-Otadui, and A. Rufer, "Analytical models of multiphase isolated medium-frequency DC–DC converters," *IEEE Trans. Power Electron.*, vol. 32, no. 4, pp. 2508–2520, Apr. 2016.

[28] N. H. Baars, J. Everts, C. G. Wijnands, and E. A. Lomonova, "Performance evaluation of a three-phase dual active bridge DC–DC converter with different transformer winding configurations," *IEEE Trans. Power Electron.*, vol. 31, no. 10, pp. 6814–6823, Oct. 2016.

[29] Y. Sang, A. Junyent-Ferré, and T. C. Green, "Transformer design in a medium voltage DC/DC converter for a DC collection network," in *Proc. 19th Eur. Conf. Power Electron. Appl.*, 2017, pp. P.1–P.10.

[30] G. G. Oggier, R. Leidhold, G. O. Garcia, A. R. Oliva, J. C. Balda, and F. Barlow, "Extending the ZVS operating range of dual active bridge high-power DC–DC converters," in *Proc. 37th IEEE Power Electron. Spec. Conf.*, 2006, pp. 1–7.

[31] B. Zhao, Q. Song, and W. Liu, "Power characterization of isolated bidirectional dual-active-bridge DC–DC converter with dual-phase-shift control," *IEEE Trans. Power Electron.*, vol. 27, no. 9, pp. 4172–4176, Sep. 2012.